Inspection of an end quenched 0.15%–0.2% C, 0.6%–0.9% Mn steel jominy bar with photothermal radiometric techniques

Yue Liu, Natalie Baddour, Andreas Mandelis, and Chinhua Wang
Center for Advanced Diffusion Wave Technologies, Department of Mechanical and Industrial Engineering, University of Toronto, 5 King's College Road, Toronto, Ontario, M5S 3G8, Canada

(Received 17 February 2004; accepted 20 May 2004)

The effect of the cooling rate on hardness and thermal conductivity in a metallurgical Jominy bar made of 0.15%–0.2% C, 0.6%–0.9% Mn (AISI 1018) steel, by means of a water end-quenched heat treatment process without diffusion-controlled case depth, is studied with photothermal radiometry (PTR). It is concluded that our two PTR techniques, common-mode rejection demodulation and conventional 50% duty-cycle square-wave frequency scan, are sensitive to low hardness values and gradients, unlike the high values all previous photothermal studies have dealt with to-date. Both PTR methods have yielded an anticorrelation between thermal conductivity and microhardness in this case as in previous cases with heat-treated and diffusion-controlled case depth profiles. It is shown that the cooling rate strongly affects both hardness and thermal conductivity in the Jominy-bar heat-treating process. © *2004 American Institute of Physics*.
[DOI: 10.1063/1.1771478]

I. INTRODUCTION

In recent years, a number of photothermal applications to hardness measurements in metals have been reported in the literature. Establishing a quantitative correlation between the microhardness and thermal conductivity or thermal diffusivity is a key issue to performing reliable photothermal hardness measurements. Various independent research groups have reported a well-established anticorrelation between thermal diffusivity/thermal conductivity and microhardness. Jaarinen and Luukkala[1] made the first attempt to study the properties of surface hardness of steel in terms of an inverse process and developed a numerical technique based on the solution of the thermal-wave equation using a two-dimensional finite difference grid. Lan *et al.*[2] used a mathematical reconstruction technique[3] to obtain the thermal conductivity depth profile of quenched steels, and found a close anticorrelation between depth dependent thermal conductivity and conventionally measured Vickers hardness. Munidasa *et al.*[4] applied the thermal harmonic oscillator[5] (THO) method on quenched steels and found an anticorrelation between thermal diffusivity and microhardness. Later, Mandelis *et al.*[6] showed that the results from investigated cold-work depth profiles in rail track samples illustrated the potential of photothermal depth profilometry as a nondestructive, noncontact inspection methodology of rail deterioration as a function of length of service in the train transportation field. From this wealth of evidence it is now established that the diffusivity depth profiles obtained for case-hardened steels anticorrelate, at least qualitatively, with destructive microhardness measurements. Fournier *et al.*[7] used a photoreflectance setup as well as a photothermal radiometric (PTR) setup to reconstruct the thermal diffusivity depth profiles of hardened steel samples. They, too, showed that there was an anticorrelation between hardness and thermal diffusivity. Walther *et al.*[8] used two different experimental methods to determine the relation between hardness and thermal diffusivity: the common laser flash technique to estimate the thermal diffusivity of a set of fully hardened, homogeneous specimens with different hardness produced by appropriate heat treatments; and lateral scanning photothermal microscopy to estimate the thermal diffusivity depth profile from localized measurements that was compared with the hardness depth profile obtained by microindentation. In general, despite the thermal-wave inverse problem types of reconstructions applied to steels and the anticorrelation trends observed between thermal diffusivity and hardness, no physical interpretation of the anticorrelated thermophysical and mechanical depth profiles (mostly for quenched steels) has been attempted. Only very recently attempts have been made to offer physical interpretations of photothermally reconstructed hardness depth profiles in processed steels. Nicolaides *et al.*[9] concluded that the depth distribution of the thermal diffusivity profile in a hardened low-alloy Mn, Si, Cr, Mo Steel (AISI 8600) is dominated by carbon diffusion during carburization, while the absolute thermal diffusivity values are dominated by microstructural changes that occur during quenching. The authors also pointed out that the validity of these conclusions for other types of steel is uncertain. Most investigations to-date have focused on samples heat treated in the presence of conventional elements, such as carbon or nitrogen, to form a concentration gradient which subsequently defines the hardness case depth profile after quenching. The effect of heat treatment on the hardness and conductivity is a combination of specific gas exposure in a furnace and cooling rate. The relationship between hardness and thermal diffusivity in carburized and carbonitrided steels has been investigated by Nicolaides *et al.*[9] and Liu *et al.*[10,11]

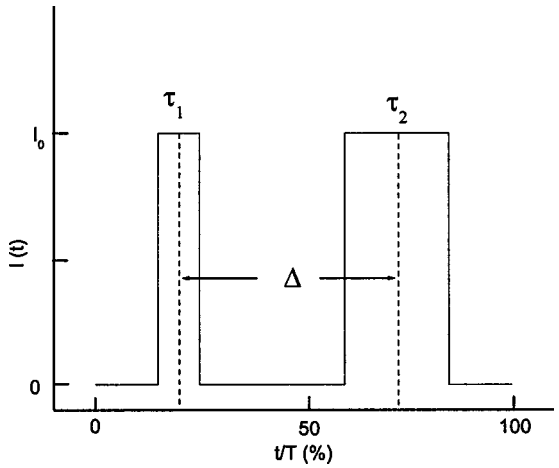

FIG. 1. Optical excitation wave form consisting of a bimodal pulse applied to the photothermal CMRD system. The horizontal time units are expressed as a percentage of a full repetition period T; τ_1 and τ_2 are the corresponding square pulse widths; Δ is the center-to-center time delay. Only one repetition period is presented for clarity.

However, the type of relationship between hardness and thermophysical properties resulting from the cooling rate of steel still remains unclear. Nevertheless, in order to perform reliable photothermal hardness tests, the sensitivity of the photothermal techniques to hardness variation is very important. To our best knowledge, all previous works[2,4,7–9] have concluded that photothermal techniques are sensitive to high hardness (maximum >800 HV and minimum >200 HV) and large hardness gradient (hardness case depth <2 mm). The applicability of photothermal methods to low hardness values (<200 HV) and gradients (case depth >2 mm) has not been studied.

In this work we used laser infrared photothermal radiometry (PTR) to explore this issue. A Jominy bar[12] made of AISI 1018 steel (0.15%–0.2% C, 0.6%–0.9% Mn) was end-quenched to form a mild hardness profile with continuously varied cooling rate along the bar with maximum hardness less than 14 HC (≈140 HV). Two types of PTR signal generation techniques were used: conventional 50% duty-cycle square-wave modulation and common-mode rejection demodulation (CMRD).[13,14] Vertical spatial scans along the side of the end-quenched Jominy bar were performed, and local hardness and thermal conductivity were measured. Measurement results from the two methods and the relationships between thermal conductivity and hardness profiles obtained from destructive mechanical measurements will be presented.

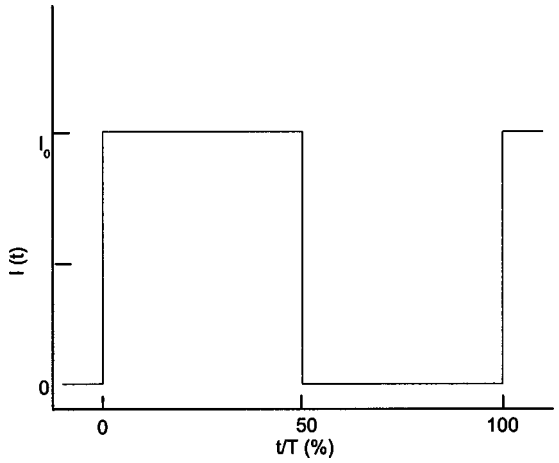

FIG. 2. Optical excitation applied to conventional 50% duty-cycle square-wave modulation in photothermal radiometry. Only one repetition period is presented for clarity.

II. LASER-BEAM MODULATION WAVEFORMS

The two-pulse configuration of the CMRD scheme is shown in Fig. 1. It has been shown[13,14] that the in-phase and quadrature demodulated lock-in outputs from any experimental system driven by such a bimodal periodic pulse excitation with period T are given by

$$Y_{IP}(f) = -\frac{2I_0}{\pi}\left\{\begin{array}{l}\cos\left(\frac{\pi\Delta}{T}\right)\left[\sin\left(\frac{\pi\tau_1}{T}\right)+\sin\left(\frac{\pi\tau_2}{T}\right)\right]\mathrm{Re}[S(f)] \\ +\sin\left(\frac{\pi\Delta}{T}\right)\left[\sin\left(\frac{\pi\tau_1}{T}\right)-\sin\left(\frac{\pi\tau_2}{T}\right)\right]\mathrm{Im}[S(f)]\end{array}\right\}, \tag{1}$$

$$Y_{Q}(f) = \frac{2I_0}{\pi}\left\{\begin{array}{l}\sin\left(\frac{\pi\Delta}{T}\right)\left[\sin\left(\frac{\pi\tau_1}{T}\right)-\sin\left(\frac{\pi\tau_2}{T}\right)\right]\mathrm{Re}[S(f)] \\ -\cos\left(\frac{\pi\Delta}{T}\right)\left[\sin\left(\frac{\pi\tau_1}{T}\right)+\sin\left(\frac{\pi\tau_2}{T}\right)\right]\mathrm{Im}[S(f)]\end{array}\right\}, \tag{2}$$

where $f=1/T$ is the CMRD wave-form repetition frequency, τ_1 and τ_2 are the two pulse widths, and $S(f)$ is the corresponding signal response of the experimental system to single-pulse excitation at the same frequency. Δ is the center-to-center time delay.

The configuration of a conventional square-wave excitation is shown in Fig. 2. The one dimensional thermal-wave signal response is given by[15]

$$S(f) = \frac{I_0(1-R)(1-i)}{\sqrt{k_{eff}\rho c\omega}} \propto \frac{1}{\sqrt{k_{eff}}}, \tag{3}$$

where ρ, c represent the material density and specific heat, respectively; I_0 is intensity of the laser beam; R is the reflectivity of the measured surface; $\omega=2\pi f$, and k_{eff} represents the depth-variable effective thermal conductivity in the range of the thermal diffusion length μ and is given by

$$k_{eff} = \frac{1}{\mu}\int_0^{\mu} k(x)dx. \tag{4}$$

From the above expressions it is clear that the corresponding signal response of the experimental system to photothermal excitation at a fixed frequency is in inverse proportion to the effective thermal conductivity, regardless of the excitation waveform.

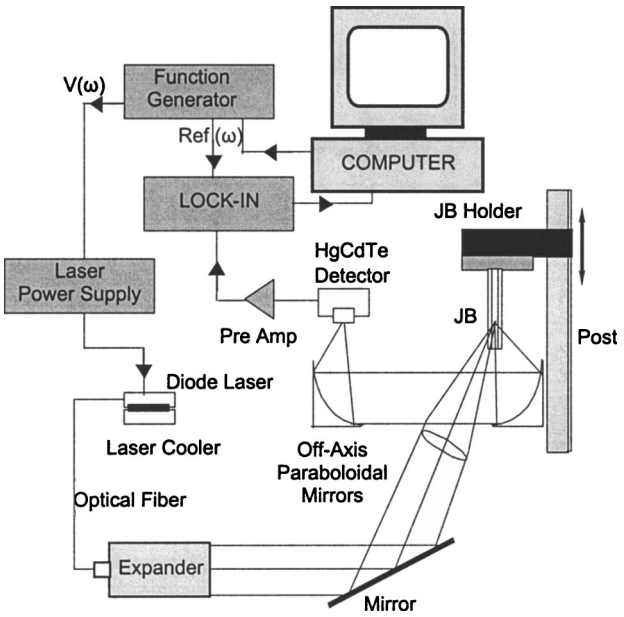

FIG. 3. Experimental setup.

III. SAMPLE PREPARATION AND EXPERIMENTAL SETUP

A. End quenching

For the end-quenching heat treatment, a portion of the 1018 AISI steel bar was cut into the form of a Jominy bar.[12] This bar was cylindrical in shape, half an inch in diameter, and 4 in. long. A flat portion was ground on one side of the bar to ensure a flat area for laser photothermal probing. The end-quench test, also referred to as a Jominy test, is widely used in the steel industry to simply and effectively determine the hardenability of a particular steel.[12] This test provides a convenient and reproducible method of quenching steel bars and determining the effect of cooling rate on the resulting hardness and microstructure. In this instance, the Jominy bar was heated in an oven at 900 °C to austenitize it for one-half hour and was then quickly transferred to a quenching jig, which directs a controlled jet of water at one end of the bar. Heat exchange between the hot steel and the water jet and heat flow occurs primarily along the length of the bar, so that the cooling rate varies from a high value at the quenched end to a low value at the far end, thus forming a continuum of hardness along the length of the bar. The Jominy curve was obtained by making Rockwell C hardness measurements along the length of the bar. The sideways flat portion was carefully polished after the quenching to keep the surface optically uniform.

B. Experimental setup

The experimental system for PTR scans is shown in Fig. 3. A high-power 20 W diode laser (Jenoptik JOLD-X-CPXL-1L) was current-modulated using a Thor Labs high power laser driver, which accepted the voltage modulation wave form from the signal function generator to modulate the laser driving current. The largely anisotropic multimode laser beam was expanded, collimated, and then focused on the surface of the sample with ≈1 mm diameter spotsize. The infrared (Planck) radiation from the optically excited sample surface was collected and collimated by two silver-coated, off-axis paraboloidal mirrors and then focused onto a liquid nitrogen-cooled HgCdTe (mercury-cadmium-telluride) detector (EG&G Judson Model J15016-M204-S01M-WE-60). The heated area of the sample was at the focal point of one mirror positioned near the sample and the detector was at the focal point of the other mirror. The HgCdTe detector is a photoconductive element that undergoes a change in resistance proportional to the intensity of the incident infrared radiation. Our detector had an active square-size area of 1 mm × 1 mm and spectral bandwidth of 2–12 μm. An antireflection coated germanium window with a transmission bandwidth of 2–14 μm was mounted in front of the detector to block any direct radiation from the laser. Prior to being sent to the digital lock-in amplifier (EG&G Instruments Model 7265), the PTR signal was amplified by a low-noise preamplifier (EG&G Judson PA101), specially designed for operation with the HgCdTe detector. The lock-in amplifier, which was interfaced with a PC, received and demodulated the preamplifier output. For CMRD measurements, the thermal-wave in-phase and quadrature lock-in signals were obtained as a function of τ_1, τ_2, and time delay Δ. In conventional 50% duty-cycle square-wave PTR measurements, thermal-wave amplitude and phase were obtained. The process of data acquisition and storage was fully automated.

IV. EXPERIMENTAL RESULTS AND DISCUSSION

As a first step, conventional PTR frequency scans were performed on the end-quenched Jominy bar. The scans were performed upwards from the quenched end, and along the bar every 0.5 cm to the middle of the bar, and then every 1 cm up to the other end of the bar. The modulated laser beam was focused at each measurement point, and the frequency was varied from 1 Hz to 2 kHz. Comparison of the full photothermal frequency scan results showed that the largest amplitude response variations in the entire frequency range appeared ≈100 Hz. The sensitivity of the technique to changes in the thermophysical properties of the steel depends on both magnitude of the thermophysical change and on geometry. When the Jominy bar was quenched, heat was transferred along the bar axially and laterally. The cooling rate at any location inside the bar was a combination of cooling rates in these two directions. Spots closest to the surface experience higher lateral cooling rate than deeper spots, due to the larger temperature gradient near the outer surface. Since the cooling rate is the dominant factor in the hardness profile formation when the chemical composition of the steel does not change, the hardness of the surface is always higher than that of the interior. Therefore, a hard surface layer ("case") is formed surrounding the bulk. From thermal-wave calculations, the frequency range corresponding to peak PTR sensitivity to hardness variations is expected to also correspond to a thermal diffusion length range commensurate with the mean case depth: At 100 Hz the thermal diffusion length is ≈200 μm when the thermal diffusivity is 14 mm^2/s.[16] Based on the foregoing results, spatial scan experiments were performed with a fixed frequency of 100 Hz.

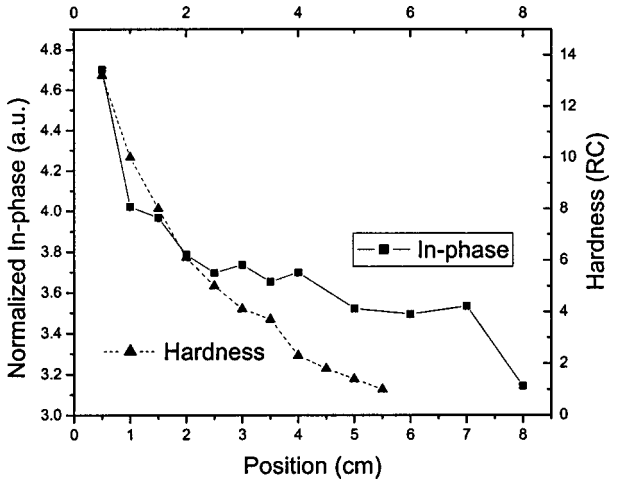

FIG. 4. Comparison of CMRD in-phase spatial scan with hardness profile. Pulse repetition rate: 100 Hz.

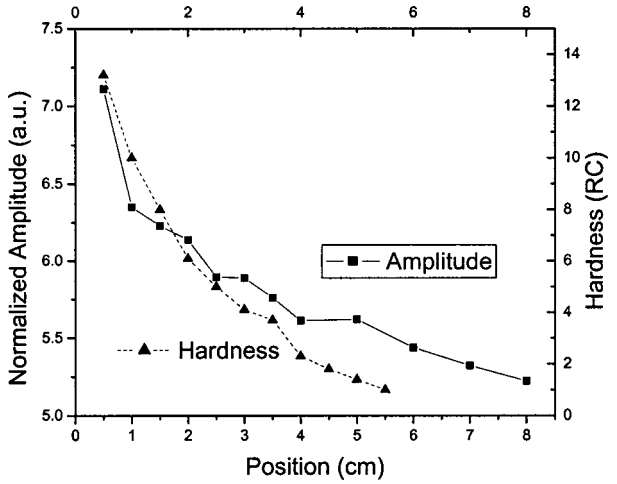

FIG. 6. Comparison of amplitude spatial scan with hardness profile. Modulation frequency: 100 Hz.

Given that the CMRD signal is a function of time delay Δ when the pulse widths τ_1, τ_2 are fixed, Fig. 1, time delay scans with 100 Hz repetition rate along the Jominy bar were performed to optimize the sensitivity of the CMRD PTR signal with respect to time delay before scanning the length of the Jominy bar side. The pulse widths were fixed at $\tau_1 = 5\%$ and $\tau_2 = 25\%$ and the center-to-center time delay Δ was varied from 15% to 85%. Upon comparison of the Δ-scan results, both in-phase and quadrature signals were found to exhibit combined optimal sensitivity at $\Delta = 17\%$. So we chose $\Delta = 17\%$ for further experiments.

Comparisons of in-phase and quadrature CMRD signal scan profiles along the side of the Jominy bar with the hardness profile from a destructive hardness test are shown in Figs. 4 and 5. Both in-phase and quadrature signals were normalized with respect to the reflectivity at each measurement spot. Both Figs. 4 and 5 show that there is a strong correlation between PTR signal and hardness. Typical error bars for both CMRD and square-wave PTR signals were estimated at 2%. Since the real (in-phase) and imaginary (quadrature) parts of the CMRD PTR signal are inversely proportional to the square root of the mean thermal conductivity as shown in Eq. (4), an anticorrelation between hardness and thermal conductivity can be obtained.

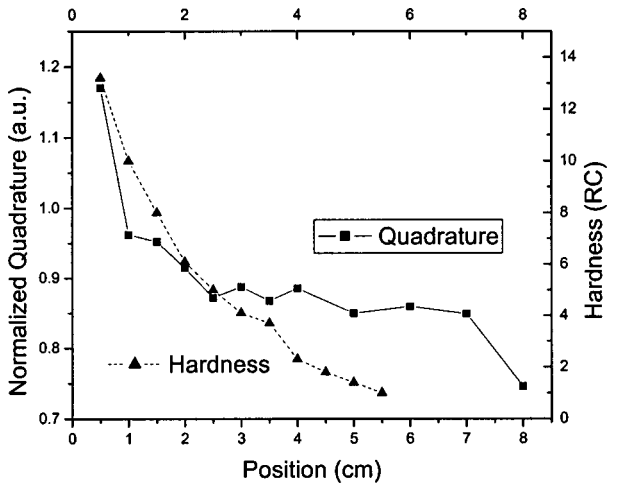

FIG. 5. Comparison of CMRD quadrature spatial scan with hardness profile. Pulse repetition rate: 100 Hz.

Figure 6 shows the results from the conventional 50% duty-cycle square-wave spatial scans compared with the independently measured hardness profile. A good correlation between the photothermal and mechanical profiles is apparent. The extent of correlation between thermal wave and hardness profiles is comparable between the CMRD and conventional square-wave scans, Figs. 4–6. The PTR phase did not exhibit as good a correlation as the amplitude, perhaps due to the very small extent of the hardness gradient normal to the surface. To reconstruct the thermal conductivity from either PTR signal, it was assumed that the thermophysical properties beyond 8 cm away from the quenched bottom of the Jominy bar were not affected by the quenching process and the thermal conductivity remained at the prequenching value of 51.9 W/mK.[17] This was based on the fact that it was not possible to obtain any measurable hardness by mechanical means (indenter) beyond 5.5 cm away from the bottom. Nevertheless, the sensitivity of PTR techniques to minute values of hardness shows a profile that keeps on decreasing past that point in Figs. 4–6. Using Eq. (3) and the PTR signal shown in Fig. 6, the effective thermal conductivity profile along the side of the Jominy bar was reconstructed. The results and comparison with the hardness profile are shown in Fig. 7. An anticorrelation between the thermal conductivity and hardness is observed, as expected. The remaining curve in Fig. 7 is the average of the thermal conductivity reconstructions of all three profiles shown in Figs. 4–6. The PTR signal definitely exhibits improved sensitivity to very low hardness profiles (<2 RC) compared to the conventional mechanical hardness measurement.

V. CONCLUSIONS

Overall, it can be concluded that the rate of quenching of this particular type of steel (AISI 1018) through cooling, in the absence of hardening through heat treating and element (carbon, nitrogen) diffusion, affects both local hardness and thermal conductivity at distances of several centimeters away from the quenched end. Experimental results from a Jominy

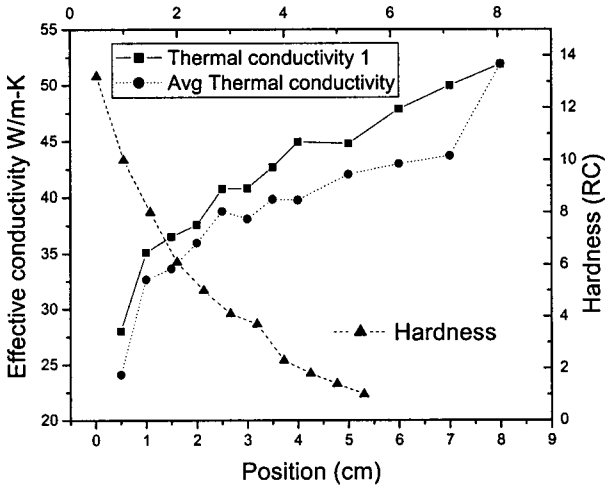

FIG. 7. Comparison of reconstructed thermal conductivity with hardness profile along the side of the Jominy bar. "Thermal conductivity 1" represents thermal conductivity profile reconstructed from amplitude spatial scan. "Av thermal conductivity" represents the average reconstructed profile from both CMRD spatial scans and the amplitude spatial scan.

bar showed that there exists an expected anticorrelation between thermal conductivity and hardness. The anticorrelation is not perfect, and this conclusion is consistent with earlier depth profilometric work from our group[4,6] and other groups.[2,8] Noncontact photothermal methods such as conventional square-wave PTR and common-mode rejection demodulation PTR can be very sensitive monitors of the case-depth-averaged local variation of hardness as a result of quenching, provided they are used judiciously by adjusting frequency and/or pulse repetition rate for matching case depth and thermal diffusion length. It is concluded that PTR techniques are sensitive to low hardness values and mild gradients, in addition to the high hardness values and steep gradients reported in all previous photothermal studies to-date.

ACKNOWLEDGMENTS

The authors wish to acknowledge the support of Materials and Manufacturing Ontario through a Collaborative Contract to A.M.

[1]J. Jaarinen and M. Luukkala, J. Phys. (Paris) **44**, C6-503 (1983).
[2]T. T. N. Lan, U. Seidel, H. G. Walther, G. Goch, and B. Schmitz, J. Appl. Phys. **78**, 4108 (1995).
[3]T. T. N. Lan, U. Seidel, and H. G. Walther, J. Appl. Phys. **77**, 4739 (1995).
[4]M. Munidasa, F. Funak, and A. Mandelis. J. Appl. Phys. **83**, 3485 (1998).
[5]A. Mandelis, J. Math. Phys. **26**, 2676 (1985).
[6]A. Mandelis, M. Munidasa, and L. Nicolaides, NDT & E Int. **32**, 437 (1999).
[7]D. Fournier, J. P. Roger, A. Bellouati, C. Boue, H. Stamm, and F. Lakestani, Anal. Sci. **17**, S158 (2001).
[8]H. G. Walther, D. Fournier, J. C. Krapez, M. Luukkala, B. Schmitz, C. Sibilia, H. Stamm, and J. Thoen, Anal. Sci. **17**, S165 (2001).
[9]L. Nicolaides, A. Mandelis, and C. Beingessner, J. Appl. Phys. **89**, 7879 (2001).
[10]Y. Liu, N. Baddour, and A. Mandelis, J. Appl. Phys. **94**, 5543 (2003).
[11]Y. Liu, N. Baddour, and A. Mandelis, J. Appl. Phys. (in press).
[12]G. Krauss, *Steel: Heat Treatment and Processing Principles* (ASM International, Material Park, Ohio, 1990).
[13]A. Mandelis, S. Paoloni, and L. Nicolaides, Rev. Sci. Instrum. **71**, 2440 (2000).
[14]S. Paoloni, L. Nicolaides, and A. Mandelis, Rev. Sci. Instrum. **71**, 2445 (2000).
[15]A. Mandelis, *Diffusion-Wave Fields: Mathematical Methods and Green Functions* (Springer, New York, 2001), Chap. 2.
[16]G. Busse and H. G Walther, in *Principles and Perspectives of Photothermal and Photoacoustic Phenomena*, edited by A. Mandelis (Elsevier Science Publishing Co. Inc., New York, 1992).
[17]*Properties of Selection: Iron, Steel of High Performance Alloys*, Metals Handbook Vol. 1, Tenth ed. (ASM International, Materials Park, Ohio, 1990), pp. 196–199.